Laser acceleration of proton bunches by petawatt chirped linearly polarized laser pulses

Yousef I. Salamin,[1,2] Jian-Xing Li,[1,*] Benjamin J. Galow,[1] Zoltán Harman,[1,3] and Christoph H. Keitel[1]
[1]*Max-Planck-Institut für Kernphysik, Saupfercheckweg 1, D-69117 Heidelberg, Germany*
[2]*Department of Physics, American University of Sharjah, POB 26666, Sharjah, United Arab Emirates*
[3]*ExtreMe Matter Institute EMMI, Planckstrasse 1, D-64291 Darmstadt, Germany*
(Received 14 January 2012; published 25 June 2012)

Detailed single- and many-particle calculations are carried out for the acceleration of protons employing linearly polarized plane-wave and tightly focused chirped laser pulses of several ten to several hundred femtosecond durations, petawatt peak powers, and relativistic peak intensities. Analytic and numerical methods of calculation are used in the single-particle cases (in vacuum), and particle-in-cell (PIC) simulations (underdense plasma) are employed in the many-particle investigations, without and with electromagnetic particle-particle interactions, respectively. The investigations cover a wide range of cases corresponding to upchirped as well as downchirped pulses.

DOI: 10.1103/PhysRevA.85.063831 PACS number(s): 37.20.+j, 52.38.Kd, 37.10.Vz, 42.65.−k

I. INTRODUCTION

Ions accelerated to energies ranging from several keV to a few hundred MeV per nucleon are useful for applications in industry [1,2], with examples including ion lithography, ion implantation, milling, and sputtering, as well as in medicine [3–7] (ion therapy). For ions to be relevant for cancer therapy, they ought to be accelerated first to energies typically in the range of 20–580 MeV/nucleon in bunches containing 10^7–10^{10} particles per bunch and with an energy spread not exceeding 1%.

Several mechanisms have been suggested for the laser acceleration of protons from various types of targets. From a solid target, like a metallic foil of micron thickness, irradiated with a powerful laser pulse, the target normal sheath acceleration (TNSA) mechanism has been suggested to explain the gain of several tens of MeV by protons [8–21] (for a recent review, see, e.g., [22]). The electrons liberated from the target by ionization of the source atoms are blown off and form a sheath of negative charge parallel to the metal surface, leaving behind them the much more massive and relatively slow-moving protons. In the space between them, the electrons and positive ions establish a strong quasistatic electric field which works to accelerate the ions in a direction perpendicular to the surface. For much thinner targets, the radiation pressure acceleration (RPA; see, e.g., the references [23–27]) or light-sail (LS) mechanisms [28–30] have been invoked to explain the process of ion acceleration. Both mechanisms assume a plasma background.

On the other hand, work on laser acceleration of ions in vacuum [31–34] has theoretically demonstrated that particle energies of several hundred MeV may be achieved using multipetawatt systems of intensity of the order of 10^{22}–10^{23} W/cm^2 focused down to subwavelength waist radii, from preionized sources. In this paper, where only linearly polarized light is employed, work will be presented whose main conclusion will be ion laser acceleration to the same energies, for the realization of which less-powerful, less-intense and not so tightly focused laser pulses are needed, provided they are appropriately frequency chirped [35–42]. Work along similar lines which employs radially polarized light may be found in Ref. [43]. We assume that the target is an ensemble of hydrogen atoms, which may be realized as a hydrogen gas target or an expanding hydrogen cluster [44]. Laser acceleration experiments with somewhat similar mass-limited targets—water spray and water microdroplet targets—have been successfully conducted before [45,46].

Four, not entirely independent, methods of calculation will be shown to lead to basically similar results for the particle exit kinetic energy, energy spread, and related features [36]. Single-particle calculations, one based on an analytic model of the chirped laser pulse and another utilizing the tightly focused pulse representation, will be presented first. This is followed by two sets of many-particle simulations: one using an initial ensemble of *noninteracting* particles uniformly distributed within a small volume but whose initial energies and positions are picked at random, and the other is a particle-in-cell (PIC) calculation. The latter is necessary because we assume an atomic source which first gets ionized by the intense laser pulse and forms an under-dense plasma of electrons and ions. The electrons get accelerated away very quickly (see Fig. 1) leaving behind them the much more massive ions which will also be accelerated to, typically, a few hundred MeV as a result of further interaction with the pulse of PW power. The improved efficiency of chirped-pulse acceleration, compared to earlier vacuum acceleration results [31–34], allows one to employ laser fields focused to larger focal waist radii equivalent to a few laser wavelengths, thus leading to intensities of the order of 10^{22} W/cm^2. Furthermore, in addition to the results presented in Ref. [36], it is found that the kinetic energies gained by chirped-pulse laser acceleration may be scaled up by increasing the pulse duration, or, the total pulse energy.

The many cases investigated demonstrate clearly that the particle exit kinetic energy scales linearly with the laser field intensity (or, equivalently, input power) and pulse duration. Proton exit kinetic energy from interaction with, for example, a 1-PW pulse of duration 350 fs and a waist radius of 2.2 μm (intensity $I_0 \sim 1.3 \times 10^{22}$ W/cm^2 [47]), can reach 250 MeV. The scaling laws, demonstrated using the plane-wave model and assuming they can be extrapolated, point to much higher exit

[*]J.X.L. is on leave from the College of Physics Science and Information Engineering, Hebei Normal University, Shijiazhuang 050016, China.

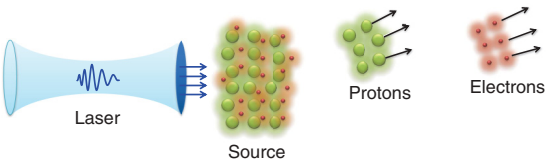

FIG. 1. (Color online) A schematic illustrating the ionization of the target atoms and subsequent acceleration of the ions and electrons, as a result of interaction with a chirped pulse.

kinetic energies. For example, a 10-PW pulse of duration 800 fs and 1.8-μm waist radius, accelerates a proton to over 8.5 GeV.

The analytic plane-wave model will be introduced in Sec. II, where expressions for the scaled momentum and energy of the particle, as well as its exit kinetic energy, will be derived as functions of a space-time variable to be chosen shortly. A clear procedure, following well-defined steps, will be devised for obtaining the optimal kinetic energy to which a particle may be accelerated, together with the corresponding optimal chirp parameter. In the same section, dependence of the optimal exit kinetic energy upon the pulse duration, and the way it correlates with the optimal chirp parameter will also be investigated. Towards the end of Sec. II, the plane-wave model will be shown to be a suitable grounds for discussion of several issues related to the process of particle laser acceleration in vacuum. For example, the conditions under which the model may work well will be briefly discussed, together with the factors that may impact its predictive power, positively and negatively. Acceleration by a tightly focused pulse will be outlined briefly and results pertaining to single- and many-particle calculations will be presented and discussed in Sec. III. Section IV will be devoted to the particle-in-cell simulations. A general discussion of all obtained results, pertaining to a 25-fs duration pulse, will be conducted in Sec. V, in addition to a test of the predictive powers of all calculational methods used, in the case of acceleration by a 350-fs pulse. Finally, an appendix is added in which a procedure is outlined for regularizing the plane-wave model pulse form, ridding its frequency spectrum of any static components that may arise from the approximate mathematical description of chirping.

II. THE PLANE-WAVE MODEL

Motion of a single particle of mass M and charge Q in the fields $\boldsymbol{E}$ and $\boldsymbol{B}$ of a laser pulse will be studied classically, but relativistically, using the Lorentz-Newton equations of motion (SI units will be used throughout this paper):

$$\frac{d\boldsymbol{p}}{dt} = Q(\boldsymbol{E} + c\boldsymbol{\beta} \times \boldsymbol{B}); \quad \frac{d\mathcal{E}}{dt} = Qc\boldsymbol{\beta} \cdot \boldsymbol{E}, \tag{1}$$

in which the relativistic energy is denoted by $\mathcal{E} = \gamma Mc^2$, and the relativistic momentum by $\boldsymbol{p} = \gamma Mc\boldsymbol{\beta}$. Also, $\boldsymbol{\beta}$ is the velocity of the particle normalized by c, the speed of light in vacuum, and $\gamma = (1 - \beta^2)^{-1/2}$ is the Lorentz factor. These equations admit analytic solutions only under very specialized conditions, such as when the fields are modeled by plane waves, as will be seen shortly. For most practically realistic conditions, only numerical solutions to the equations are possible.

A. An analytical model

Since the laser pulse in our calculations will be assumed to be focused to a waist radius $w_0 > \lambda_0$, where λ_0 is the unchirped wavelength, a model that contains plane-wave characteristics, to be highlighted shortly, turns out to be sufficient for its description. The purpose of introducing this model is threefold. First, its simplicity will allow it to serve as a basis to elucidate and intuitively understand the process of ion acceleration by a frequency-chirped pulse. Second, it will be used to benchmark the parameters that will be later employed within the context of a more realistic approach, one in which the laser pulse is modeled in terms of tightly focused fields. Finally, details and a discussion of relevance to the mechanism of acceleration, will be presented for which not enough space has been devoted elsewhere [36].

With propagation along the $+z$ axis and polarization along x, the electric and magnetic fields of the pulse may be written as

$$\boldsymbol{E} = \hat{\boldsymbol{x}} E_0 f(\eta), \tag{2}$$

$$\boldsymbol{B} = \hat{\boldsymbol{y}} \frac{E_0}{c} f(\eta), \tag{3}$$

where E_0 is a constant amplitude, $\eta = \omega_0(t - z/c)$, and $\omega_0 = 2\pi c/\lambda_0$ is the unchirped angular frequency (corresponding to the *unchirped* wavelength λ_0). Note that for it to represent a traveling pulse, f ought to be written as some carrier wave, like $\cos(\eta + \phi_0)$, where ϕ_0 is a constant *initial* phase, and a pulse envelope, such as a Gaussian $g(\eta) = \exp(-\eta^2/2\sigma^2)$, where σ is a full width at half maximum (FWHM) in η space for the Gaussian envelope [see Eq. (4) below, in which τ is the pulse duration, or *temporal FWHM*]. Thus, the fields above clearly carry plane-wave characteristics, despite having finite extension in space and time, and satisfy Maxwell's equations manifestly. Purely plane-wave fields have infinite space-time extension and are ideal at best, whereas those given by Eqs. (2) and (3) are much closer to a realistic representation, provided the pulse duration is not too large.

A linear frequency chirp amounts to letting $\omega_0 \to \omega(\eta) = \omega_0(1 + b\eta)$ in $f(\eta)$, where b is a dimensionless chirp parameter. This immediately turns $\cos(\phi_0 + \eta)$ into $\cos(\phi_0 + \eta + b\eta^2)$ and leaves $g(\eta)$ unchanged. So, in Eqs. (2) and (3) we take for f the following function:

$$f(\eta) = \cos(\phi_0 + \eta + b\eta^2)e^{-\eta^2/2\sigma^2}; \quad \sigma = \frac{\omega_0\tau}{2\sqrt{2\ln 2}}. \tag{4}$$

Note that chirping the frequency in the manner described above leads necessarily to *chirping* other laser parameters. Thus, one has a *chirped* wavelength $\lambda(\eta) = 2\pi c/\omega(\eta) = 2\pi c/[\omega_0(1 + b\eta)] = \lambda_0/(1 + b\eta)$. Even in this *plane-wave* model, a beam waist radius will be needed, as it enters into the calculation of the peak intensity I_0 from the peak power P_0, through

$$P_0 = \tfrac{1}{2}\pi w_0^2 I_0; \quad I_0 = \tfrac{1}{2}c\varepsilon_0 E_0^2, \tag{5}$$

where ε_0 is the permittivity of free space. In this connection, a first assumption will be made, namely, that the diffraction angle $\varepsilon = \lambda/(\pi w_0)$, to be used in Sec. III, remains fixed throughout. So, writing the *unchirped* waist radius as $w_0 = \alpha\lambda_0$, where α is a constant of proportionality, its *chirped* counterpart will

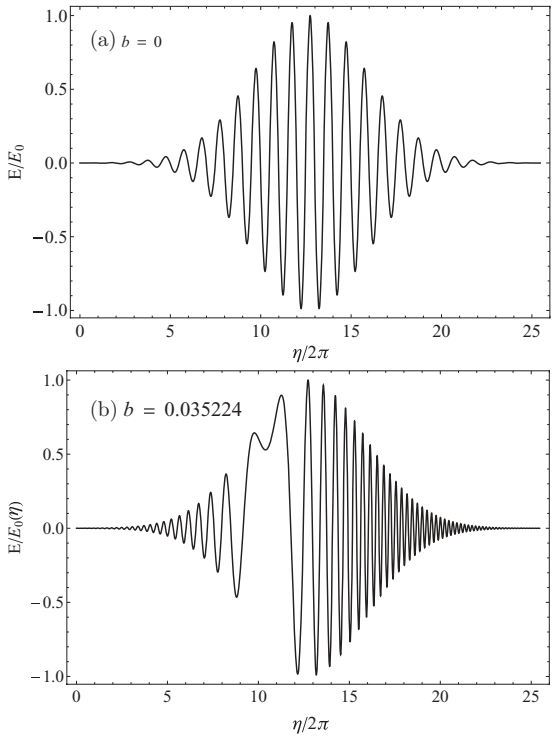

FIG. 2. Shifted ($\bar{\eta} = 4\sigma$) normalized electric field of the *plane-wave* Gaussian pulse of duration $\tau = 25$ fs and waist radius $w_0 = 1.8\lambda_0$ [introduced here solely for the purpose of calculating the peak intensity from Eq. (5)]. (a) Unchirped field. (b) Chirped field with $E_0(\eta) = E_0(1 + b\eta)$.

be $w_0(\eta) = \alpha\lambda(\eta) = \alpha\lambda_0/(1 + b\eta) = w_0/(1 + b\eta)$. Furthermore, it will be assumed that the peak power P_0 will be fixed, as will be the case throughout this paper, so that Eq. (5) suggests that the peak amplitude E_0 ought to be replaced by a *chirped* amplitude:

$$E_0(\eta) = \frac{2}{w_0(\eta)}\sqrt{\frac{P_0}{\pi c\varepsilon_0}} = \frac{2}{w_0}\sqrt{\frac{P_0}{\pi c\varepsilon_0}}(1 + b\eta). \\ = E_0(1 + b\eta). \tag{6}$$

To ensure that a particle, starting from rest at $z = 0$, will interact with the entire pulse, a shift by $\bar{\eta}$ will be introduced to η. In other words, one lets $\eta \to \eta - \bar{\eta}$, everywhere. Effectively, this shifts the center of the pulse from $\eta = 0$ to $\eta = \bar{\eta}$, without changing any of its parameters or influencing the dynamics of the particle with which it interacts. So, technically, the shift is not needed at all, but it does tie in consistently with our choice of initial conditions, to be made shortly, in presenting an intuitively clear picture.

In Fig. 2, the normalized electric field of the pulse is shown in its shifted form (with $\bar{\eta} = 4\sigma$). Figure 2(b) shows the field of a pulse with positive chirp corresponding to a dimensionless parameter $b = 0.035224$. It exhibits clearly a quasistatic portion, which we believe is responsible for the process of particle acceleration. Interaction of the particle with this portion of the field results in nonzero energy gain, whereas interaction with the remaining wings on the right and left, the symmetry of which is not broken so severely, leads to very little gain, if at all. This issue will be discussed in more detail below.

As has recently been shown elsewhere [36] when the fields (2) and (3) are substituted in Eq. (1), the latter break up into four component equations from which two constants of the motion could be identified immediately. For particles born at $t = 0$, at rest near the origin of coordinates, the constants of the motion are $\gamma\beta_y = 0$ and $\gamma(1 - \beta_z) = 1$. With the help of the constants, it can easily be shown that

$$\gamma\beta_x(\eta) = a\int_{\eta_0}^{\eta}(1 + b\eta')f(\eta')d\eta'; \quad a = \frac{QE_0}{Mc\omega_0}, \tag{7}$$

where $\eta_0 = 0$, for the adopted initial conditions, and a^2 may be taken essentially as a dimensionless intensity parameter for the laser system employed. Using these parameters, an expression for $\gamma\beta_x(\eta)$ may be obtained exactly in terms of error functions. With the knowledge that including it here may serve no practical purpose, the expression will be left out.

On the other hand, evolution in η of the energy of the particle, scaled by its rest energy Mc^2, may be found from

$$\gamma(\eta) = 1 + \tfrac{1}{2}(\gamma\beta_x)^2. \tag{8}$$

Hence, an expression for evolution of the kinetic energy of the particle follows trivially from

$$K(\eta) = \frac{Mc^2}{2}(\gamma\beta_x)^2. \tag{9}$$

Expressions for other aspects of the particle dynamics, such as its momenta and trajectory equations, may also be derived, sometimes in exact analytic forms.

B. Exit particle kinetic energy

Of particular importance to us, in this paper, is the exit particle kinetic energy which, in principle, may be calculated from Eq. (9) for a suitably large value of the upper limit on the integration ($\eta \to \eta_f$). The program of calculating a desired exit kinetic energy, employing a given set of laser system parameters, starts with a plot, like the one given in Fig. 3, of the exit kinetic energy $K(\eta_f)$, as a function of the dimensionless chirp parameter b. Three features of Fig. 3 are obvious. The first concerns the approximate left-right symmetry about $b = 0$, or the symmetry between positive and negative chirping, at least for the parameter set used. Note that the unshifted and unchirped field is an even function of η and that the *evenness* is broken only slightly by introduction of a small chirp parameter b. The second feature to show clearly in Fig. 3 is the flat near-zero portion in the middle, about $b = 0$. This agrees well with the Lawson-Woodward theorem, according to which no energy can be gained by a particle from interaction with an unchirped plane-wave field in vacuum and in the absence of other externally applied fields or boundaries. Finally, consider the existence of maxima and minima in the $K(\eta_f)$ versus b plot. Closer scrutiny reveals that for b values that produce a quasistatic portion, similar to that shown in Fig. 2(b), the particle gains maximum energy, as its motion gets synchronized with the radiation field. Total lack of synchronization, on the other hand, leads to no energy gain [a minimum in the $K(\eta_f)$ versus b plot].

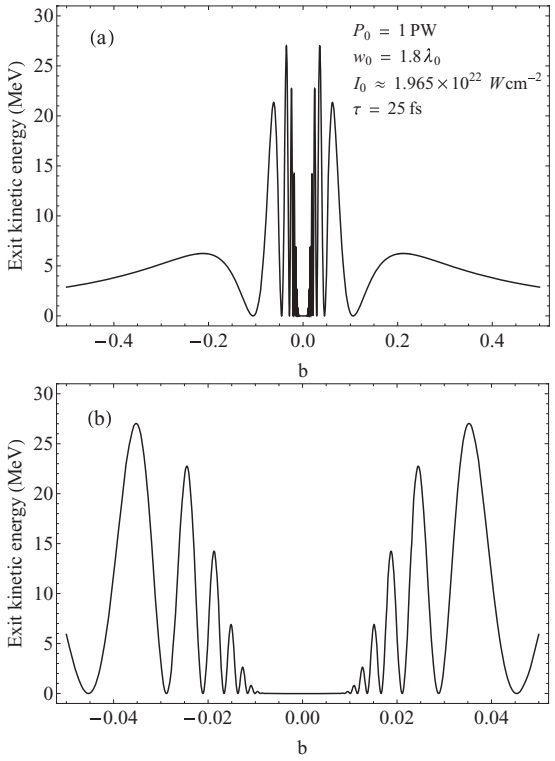

FIG. 3. Single proton exit kinetic energy as a function of the dimensionless chirp parameter b. The proton is assumed initially at rest at the origin of coordinates and is subsequently accelerated by a laser system of peak power P_0 and peak intensity I_0, and modeled by a finite Gaussian pulse of duration τ and focused to a waist radius w_0. In the calculations, a shift of $\bar{\eta} = 4\sigma$ and $\eta_f = 8\sigma$, have been used. (b) Merely a zoom-in on the central part of (a).

The absolute maximum exit kinetic energy of a particle will, henceforth, be denoted by $K^*_{\rm exit}$, and the corresponding value of b for which this energy is achieved will be called *the optimal chirp parameter* , to be denoted by b^*. For example, in Fig. 3, $b^* = 0.035224$, which has already been used to produce Fig. 2(b). For the given set of parameters, $K^*_{\rm exit} \simeq 27$ MeV.

Evolution of the kinetic energy with η, throughout the interaction between the particle and the pulse, is also quite interesting. This is shown in Fig. 4, for the case of $b^* =$

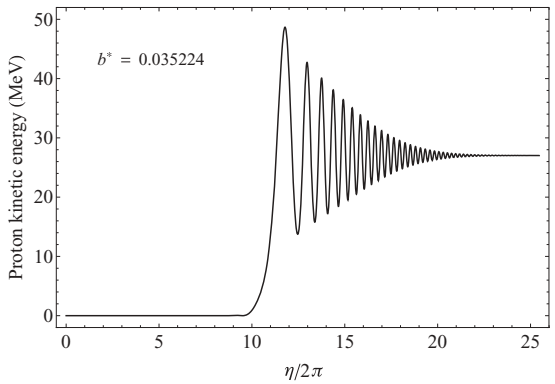

FIG. 4. Single-proton's kinetic energy evolution, as a function of $\eta/2\pi$, as it interacts with a chirped laser pulse. Initial conditions and all laser parameters are the same as in Fig. 3.

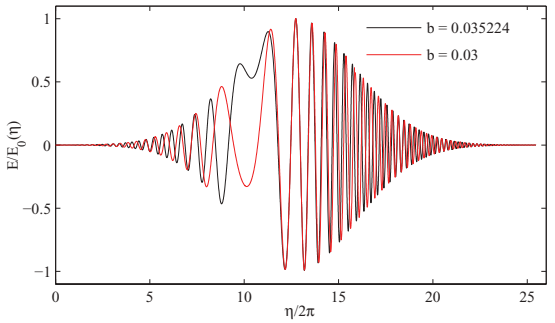

FIG. 5. (Color online) Normalized chirped electric field of the plane-wave Gaussian pulse of duration $\tau = 25$ fs for optimal $b^* = 0.035224$ (black) and for $b = 0.03$ (red or light gray).

0.035224. Note that interaction with the not-so-distorted wings of the pulse results in very little energy gain by the particle, as has already been inferred above, while most of the appreciable gain comes from interaction with the quasistatic part to the left of the center of the pulse [compare Fig. 4 with Fig. 2(b)].

Figure 3 shows that the exit kinetic energy $K(\eta_f)$ is rather sensitive to small variations of the parameter b near the maxima. A question may potentially arise as to whether this dependence upon b would complicate the experimental generation of the required chirped pulses. To answer this question, it should be recalled that b has been merely introduced as a parameter to mathematically describe a pulse shape having broken symmetry, manifesting in the quasistatic component, which results in substantial energy gain. In Fig. 5, one can see that two close values of the chirp parameter (for optimal $b^* = 0.035224$ and for $b = 0.03$) lead to completely different pulse shapes. Experimentally, every pulse is defined by its temporal shape or by its spectrum. To generate such a pulse, one ought to synthesize it by its particular spectrum. Due to the implicit meaning of b, we do not expect sensitive dependence of the acceleration scheme on b to hinder an experimental realization.

C. Optimizing the particle's exit kinetic energy

To investigate ways of optimizing it, the exit kinetic energy dependence upon several factors will be investigated next. Variation of the kinetic energy with the *peak intensity* $I_0 = 2P_0/(\pi w_0^2)$ and, hence, with the peak power P_0, is trivial. Note that Eqs. (7)–(9) clearly show that the kinetic energy of the particle varies linearly with $a^2 \propto E_0^2$. Thus, it follows that the particle's scaled energy varies linearly with the peak intensity (or, equivalently, with the peak power) of the laser system employed. Likewise, the scaled energy varies linearly with the ratio $(Q/M)^2$.

On the other hand, variation of the particle's energy with the pulse duration is not as straightforward to investigate from the equations above, but will turn out to be *numerically* simple, too. Effect of the pulse duration τ propagates through the equations above via σ, which is proportional to τ. However, a longer pulse means longer particle-field interaction times, thus making available to the particle many more photons to absorb from during interaction. So, it is plausible to expect the exit particle kinetic energy to increase with increasing pulse duration. To test this hypothesis, elaborate calculations have

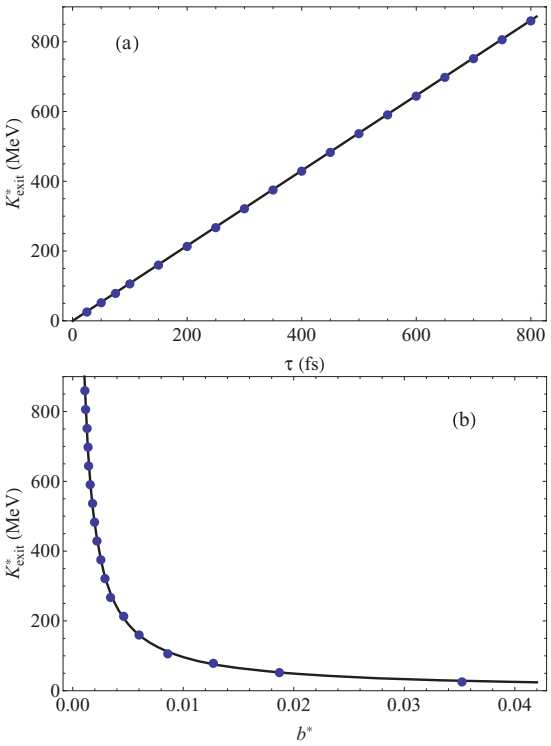

FIG. 6. (Color online) Maximum proton exit kinetic energy as a function of (a) the pulse duration τ, and (b) the optimal chirp parameter b^*. Everywhere in this figure, the peak power, the waist radius at focus, and the initial conditions are the same as in Fig. 3. The continuous lines are best fits to the data points shown by solid circles.

been performed whose results are displayed in Fig. 6(a). Note that, at least for the range of τ values considered in Fig. 6, the maximum exit kinetic energy attainable by the particle is clearly proportional to the pulse duration ($K^*_{\rm exit} \propto \tau$).

Furthermore, it can be seen quite clearly that the *global maximum exit kinetic energy* is inversely proportional to the optimal chirp parameter (i.e., $K^*_{\rm exit} \propto 1/b^*$) [see Fig. 6(b)], in which only upchirped cases have been considered.

We close this subsection by making some order-of-magnitude estimates based on extrapolation of the exit kinetic energy dependencies considered above, and taking into account current and/or envisaged laser technology developments. The validity of the model becomes increasingly in doubt with increasing pulse duration, therefore, we consider a 10-PW peak-power laser system with a beam-waist radius $w_0 = 1.8\ \mu$m. The peak intensity that would be made available for particle acceleration from this system is $I_0 \sim 1.965 \times 10^{23}\ {\rm W/cm^2}$. Assuming that the direct proportionality between $K^*_{\rm exit}$ and the peak power (or peak intensity) still holds true for these parameters, then work along lines similar to the above lead to the prediction that a proton may gain $K^*_{\rm exit} > 8.5$ GeV, following interaction with an 800-fs duration pulse. Recall that the pulse energy, calculated approximately from multiplying the power with the pulse duration, would be ∼8 kJ, in this case. Laser systems having specifications of relevance to this case are now within reach [48,49].

D. Further considerations and issues

The finite-duration plane-wave pulse model discussed in this section is not entirely without shortcomings, at the conceptual and intuitive levels. To begin with, ultrapowerful laser systems deliver short and tightly focused pulses. To represent such pulses realistically, a Gaussian description is most suitably used. As is well known, a tightly focused Gaussian beam is planar only at points too far away from the focus, and on the plane through the focus and perpendicular to the direction of propagation. The plane-wave model works so well because interaction between the particle and pulse occurs mostly near the focus. The predictive power of the model is also enhanced when focusing is not so tight ($w_0 \gg \lambda_0$). Under these conditions, one need not retain high-order terms in the description of the fields beyond the paraxial approximation. Slightly beyond the plane through the focus, validity of the plane-wave model becomes doubtful especially for short (few-cycle) and tightly focused ($w_0 < \lambda_0$) pulses.

An important issue needing discussion here is related to the part of the pulse we have described as being quasistatic in Fig. 2(b). This visible feature actually points to the existence of a zero-frequency component in the spectrum of the pulse. Closer scrutiny reveals that the chirped frequency indeed vanishes identically for $\eta^* = -1/b^* + \bar{\eta}$. For the case discussed above, $\eta^*/2\pi \simeq 8.21$. Assuming that a severe frequency chirp, such as has been considered in this work, can be realized experimentally, the zero-frequency and related issues can still be circumvented. Calculations, whose details will be relegated to the appendix, demonstrate that a small band of frequencies, centered on the zero-frequency component, can always be filtered out without affecting the particle energy gain appreciably, as is shown clearly in Fig. 7.

Intimately related to this issue is the nonvanishing of the time integral of the electric field in Eq. (4) over the entire pulse. Note first that the filtering process alluded to above lowers the absolute value of the integral and makes it approach zero. On the other hand, low-amplitude negative wings may be added to the pulse, on the left- and right-hand sides, to render the vanishing of the integral possible.

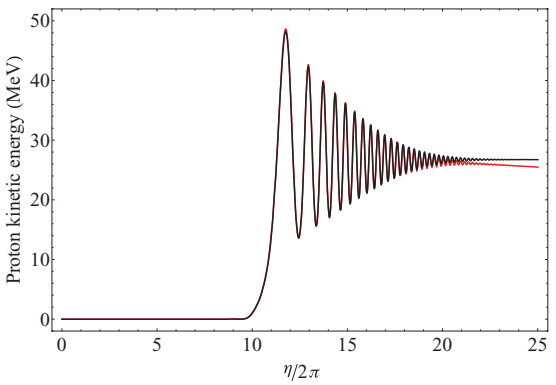

FIG. 7. (Color online) Single-proton's kinetic energy evolution, as a function of $\eta/2\pi$, as it interacts with a chirped laser pulse with the zero-frequency component (black) and without it (red or light gray). The filter width (see appendix) is $\Delta = 0.0002$, and the initial conditions and all laser parameters are the same as in Fig. 3.

III. ACCELERATION BY A TIGHTLY FOCUSED PULSE

Strictly speaking, the particle spends some time engulfed by parts of the pulse that are beyond the plane through the focus. Deviation from the plane-wave character in those regions, especially with tight focusing, forces upon our investigations a representation for the fields more realistic than the plane-wave description. The choice for further investigations will be the generalized Lax series, according to which the electric field has three components and the magnetic field has two [50]. The field components will contain terms of order $O(\epsilon^4)$, where ϵ is the diffraction angle of the Gaussian-beam model. Stopping at terms of $O(\epsilon^4)$ seems to suffice in light of the fact that $\epsilon = 1/1.8\pi \simeq 0.1768 \ll 1$, for the parameters used. Each component will also be multiplied by a Gaussian envelope similar to the one employed in the plane-wave model. In the tightly focused case, the equations of motion (1) cannot be solved analytically. Rather, they will be solved numerically, subject to the same initial conditions as has been used in the plane-wave case. Results from both models will be compared and contrasted. By contrast, the radially polarized work presented elsewhere [43] does not involve any plane-wave-based analysis.

A. Single-particle calculations

Dynamics of a single proton in the tightly focused Gaussian laser pulse will be investigated first. Working numerically, but along the same lines as was done in the plane-wave case, Fig. 8 has been produced employing the parameters of Fig. 3. The two figures exhibit similar structures and comparable general features. However, values of b that correspond to exit kinetic energy maxima and minima differ significantly. For example,

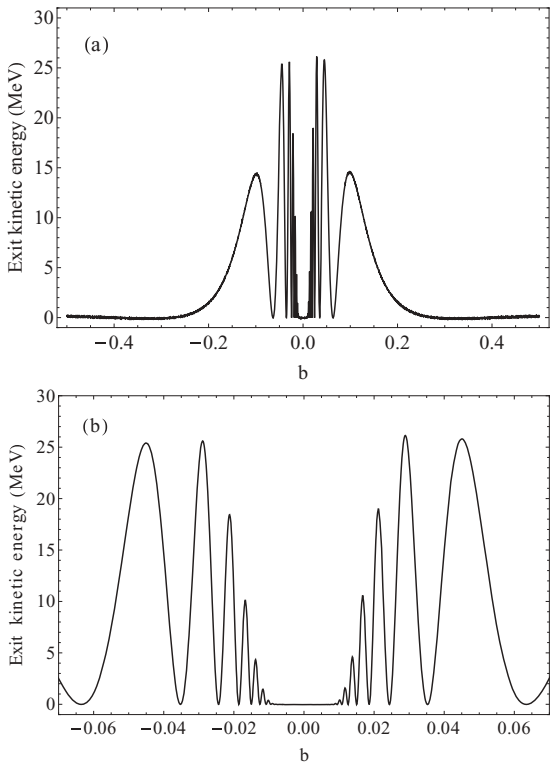

FIG. 8. Same as Fig. 3, but for a tightly focused laser pulse.

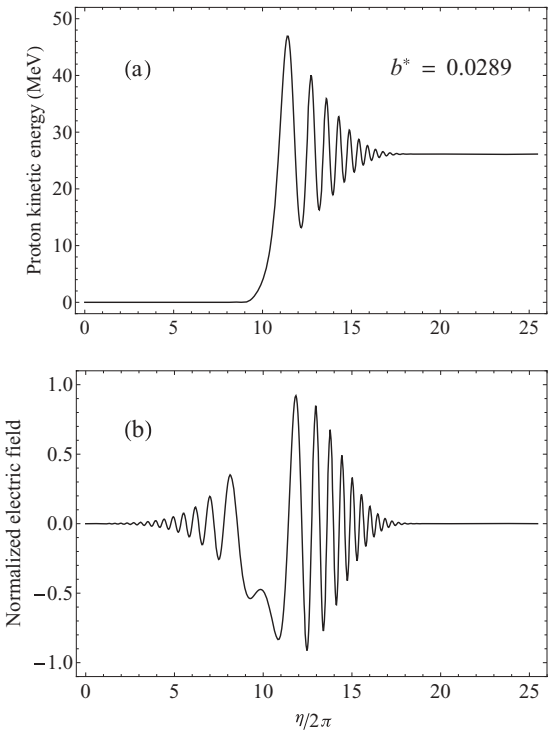

FIG. 9. (a) Same as Fig. 4, but for a tightly focused laser pulse. (b) Normalized electric field component $E_x/E_0(\eta)$, where $E_0(\eta) = E_0(1 + b\eta)$, sensed by the proton whose kinetic energy evolution is shown in (a) during interaction with the pulse.

the global maximum in Fig. 8(b) is $K^*_{\text{exit}} \simeq 26$ MeV (compared to 27 MeV in the plane-wave model) and occurs at $b^* \simeq 0.0289$ (compared to 0.035224 in the plane-wave case).

Figure 9(a) shows evolution in η of the proton kinetic energy during interaction with a chirped tightly focused 1-PW laser pulse of duration $\tau = 25$ fs. For the chirp parameter $b^* = 0.0289$, Fig. 9(a) exhibits features of the case leading to the global exit kinetic energy maximum of 26 MeV, and should be compared with Fig. 4 of the corresponding plane-wave case. Apart from minor details, the two figures exhibit identical features.

In Fig. 9(b), the normalized electric field component $E_x/E_0(\eta)$ sensed by the proton along its trajectory is shown. This is slightly different from Fig. 2(b) of the plane-wave case in that, among other things such as the chirp parameter, its frequency is Doppler shifted due to the fact that the particle is fast moving. Note that the field sensed by the proton exhibits a quasistatic portion due to the frequency chirp. Here, too, interaction with the quasistatic part results in a substantial jump in the particle's kinetic energy, followed by an oscillatory part due to interaction with the high-frequency portion of the pulse to the right. Note that the *accelerating part* of the pulse is negative [unlike in the plane-wave case; see Fig. 2(b)]. This is due to the fact that the leading term in E_x of the focused field is a sin function (not a cos function) and contains one Guoy phase. These two points make up for a total phase difference of π between the plane-wave and tightly focused fields. The overall effect of this π-phase difference on the particle motion will (here) simply be that projection of its trajectory onto the xz plane, after exiting the interaction region, will be below the

z axis. Alternatively, one can simply insert by hand a nonzero value $\phi_0 = \pi$ for the initial phase in the expression giving E_x and bring about qualitative agreement between Figs. 2(b) and 9(b) and the corresponding trajectories.

B. Many-particle calculations

The single-particle calculations are of very limited utility, in light of the fact that applications require simultaneous acceleration to the desired energies of many particles, tens of millions per bunch in the case of ion therapy, for example. The basic equations needed to investigate the many-particle dynamics are the same [Eq. (1)]. The initial conditions on position, however, will be different in general for the different particles. To be specific, dynamics of $N = 3000$ *noninteracting* particles will be investigated. Initially, the particles will be assumed stationary and randomly distributed within a cylinder (of length $L = 0.2\lambda_0$ and radius $R = 0.3\lambda_0$) centered about the origin of coordinates and oriented along the direction of propagation of the laser pulse (the z axis). The fields will also be the same as in the single-particle calculations, the generalized Lax series expressions to $O(\epsilon^4)$. Many-particle simulations will next be described and their results discussed.

Two sets of plots are shown in Fig. 10. The column on the left displays four snapshots of the projection of the ensemble of protons, assumed noninteracting, onto the xz plane, that on the right is similar, albeit for the projection onto the xy plane. It should be borne in mind that, initially ($\eta_0 = 0$), the xy cross section is circular (radius $0.3\lambda_0$ and center at the origin of coordinates) and the xz cross section is rectangular (dimensions $0.2\lambda_0 \times 0.6\lambda_0$). Recall also that σ is a dimensionless parameter in terms of which η is expressed. For example, the pulse, in the example considered, extends over values of η ranging between zero and 8σ (for a particle initially at $z = 0$) and so does its interaction with the particle. For a pulse of duration $\tau = 25$ fs, $\sigma \simeq 17$. Thus, the instant at which the snapshots shown in the second row of plots in Fig. 10 approximately marks the end of the particle-laser interaction. Beyond that time the particles move in vacuum in a nearly field-free region, in straight lines whose directions depend crucially upon the histories of their individual interactions during the time corresponding to the interval $\eta_0 = 0$ to $\eta = 8\sigma$. That is why the particle distribution gets distorted and grows in size with time, despite neglecting the particle-particle Coulomb repulsions. For example, the center of the distribution gets displaced transversely by $\Delta x \simeq 72.3\lambda_0$ and axially by $\Delta z \simeq 8\lambda_0$. So, roughly speaking, it emerges at some angle $\phi \simeq \arctan(72.3/8) \simeq 84^\circ$. On the other hand, the center of the distribution does not seem to move away from $y = 0$, mostly because E_y is the weakest of the three electric field components of the pulse.

Depending on each particle's individual initial positions within the ensemble, their trajectories evolve differently and the distribution of protons gets distorted and spreads out. It is, therefore, appropriate to talk about mean values and the corresponding spreads for the particle dynamics. Thus, one may introduce the mean exit kinetic energy $\bar{E}_{\rm exit}$ of the ensemble and the spread $\Delta E_{\rm exit}$ in it, as a result of interaction with the pulse. For the distribution described above, $\bar{E}_{\rm exit} \simeq 25.95 \pm 0.12$ MeV, which agrees quite well with our single-particle calculations.

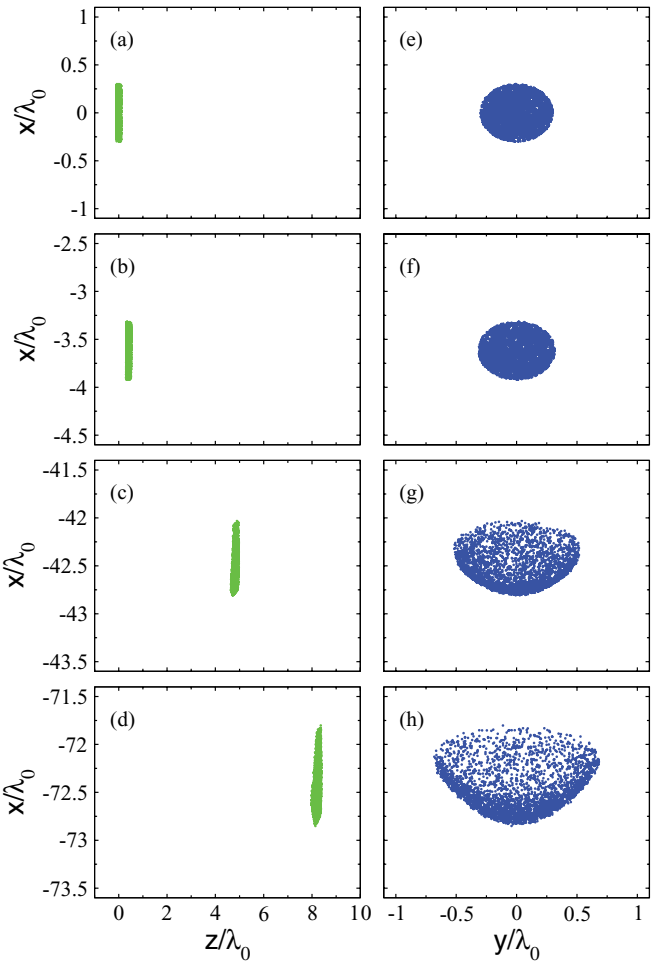

FIG. 10. (Color online) Evolution in time of an ensemble of 3000 noninteracting protons, initially at rest and randomly distributed within a cylinder of length $L = 0.2\lambda_0$ and radius $R = 0.3\lambda_0$, centered at the origin of a Cartesian coordinate system and whose axis is oriented along z. (a)–(d) Snapshots of the projection of the evolving ensemble onto the xz plane; (e)–(h) snapshots of the projection onto the xy plane. Top to bottom, the pairs of snapshots are for times corresponding to values of the variable η equal to 0σ, 8σ, 60σ, and 100σ, respectively.

These many-particle simulations also allow one to test if the acceleration scheme is stable against fluctuations of the laser parameters such as pulse duration, phase, and power. We have found that larger variations, on the 10% level in the pulse duration and power, change the resulting exit kinetic energies up to 15%, and the variations in the initial phase up to 10° have a negligible effect. In all cases, the energy spread for a given pulse stays below 1%. Additionally, we performed simulations assuming the particle ensemble to have a nonzero initial kinetic energy. The ensemble is assumed to move along the polarization direction (x direction) of the laser. For a low initial kinetic energy of 10 ± 1 keV, the resulting energy changes only slightly. Low initial kinetic energies are characteristic for, for example, a supersonic hydrogen gas jet target. For higher initial kinetic energies, for example, 100 ± 10 keV, the resulting exit kinetic energy of the ensemble decreases by 12.5%, while its energy spread increases but still remains on the 1% level.

IV. PARTICLE-IN-CELL (PIC) SIMULATIONS

Two of the assumptions made about the ensemble of protons discussed above are not very realistic. Protons interact and their mutual repulsion cannot be neglected entirely. Thus, spreading of the distribution will be more than that estimated above when the particle-particle interactions are taken into account. On the other hand, while one may think of the bunch of protons as produced from, say, ionization of an ensemble of hydrogen atoms, and are then guided electrostatically to be irradiated with the laser pulse, going one step backwards in time is more realistic. Taking as a source for the protons a preionized hydrogen plasma or a preionized expanding hydrogen cluster [44], forces upon the investigation the need to take the dynamics of the electrons into account. In this section, such a scenario is considered and the dynamics will be analyzed employing particle-in-cell simulations. The particle-particle interaction effects are taken care of in the simulations. Following laser-assisted ionization of the source atoms, the electrons are blown off and leave the scene quickly, leaving behind them the much more massive, and relatively slow-moving, protons. The protons then acquire energy from interaction with the pulse and get accelerated as well.

The spatial resolution of our simulation box is given by $\Delta z = \Delta x = \lambda_0/100$, where the laser wavelength is $\lambda_0 = 1\ \mu$m. The quasiparticle number per cell is 100, for both protons and electrons. The x-polarized laser pulse enters the simulation box from the left and propagates in the z direction. For the fields we choose those of the plane wave given in Eqs. (2) and (3), suitably modified by chirping and shifting everywhere. The target is assumed to be a 2D preionized plasma cell of length $0.2\lambda_0$ in the laser propagation (z) direction, and extension $0.6\lambda_0$ in the transverse (x) direction. Here, we assume the electrons (in the hydrogen gas) to be underdense (number density $n_e = 0.1n_c$, where $n_c = 1.1 \times 10^{21}\text{cm}^{-3}$ is the critical density for the $\lambda_0 = 1\ \mu$m wavelength). For the protons, the total number being accelerated corresponds to $\sim 10^7$ per bunch. The laser power employed has been $P_0 = 1$ PW, which corresponds to a laser peak intensity $I_0 \sim 1.965 \times 10^{22}$ W/cm^2 for a waist radius $w_0 = 1.8\lambda_0$. Finally, the pulse duration is $\tau = 25$ fs and the dimensionless chirp parameter is $b = 0.035224$.

Results from the PIC simulations are displayed in terms of 2D particle density distributions in Fig. 11. Displayed are snapshots taken at calculation times corresponding to 8, 26, 192, and 318 laser field cycles, respectively. So, for the purpose of comparison with Figs. 11(a)–11(d) note that 8σ is equivalent to 25.4620 field cycles, 60σ to 190.9652 cycles, and 100σ corresponds to 318.2753 cycles. In (a) whose instant approximately coincides with the end of the first one-third of the total particle-pulse interaction time, one can see clearly that the electrons have been detached and are moving separately from the protons. The electron density variations are also visible in (a) and they exhibit oscillations which reflect the oscillatory nature of the accelerating field. Figures 10(b)–10(d) and 11(b)–11(d) correspond to like times and can, therefore, be compared and contrasted in some respects, despite the fact that they are drawn to different scales. Note that the electrons have already left the picture and are followed no more after Fig. 11(a). The time of the snapshot shown in (b) roughly marks

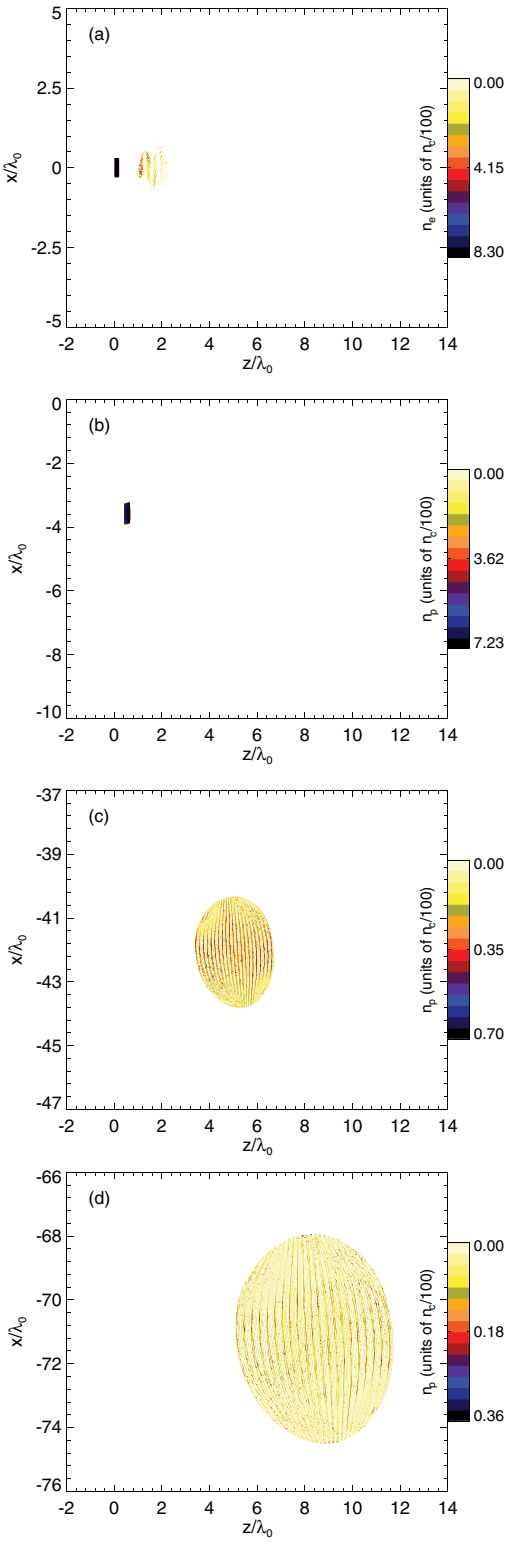

FIG. 11. (Color online) Snapshots of the electron and proton density distributions during and after interaction with a plane-wave pulse whose parameters are the same as in Fig. 9, at times corresponding to values of η equal to 2.5σ,8σ,60σ, and 100σ, respectively. The electron distribution is out of range and absent from (b)–(d). The initial distribution is two-dimensional (in the xz plane). Note the change of scale in reading Figs. 10 and 11 together.

the end of interaction with the pulse. From (b) to (d) motion is only governed by the momentum gained from interaction with the pulse, which has just been terminated, and the particle-particle Coulomb repulsion, which shows its influence in the expanding proton distribution. Several quantities may be estimated for the proton distributions shown in Fig. 11. First the distribution has grown transversely by $\delta x \simeq 6.9\lambda_0$ (from $0.6\lambda_0$ to $\simeq 7.5\lambda_0$) and $\delta z \simeq 6.3\lambda_0$ longitudinally (from $0.2\lambda_0$ to $6.5\lambda_0$). Second, the center of the distribution has roughly been displaced by $72\lambda_0$ transversely and $8\lambda_0$ longitudinally. This last set of data shows that the center of the distribution has undergone a deflection of $\phi = \arctan(9) \simeq 84^\circ$ below the pulse propagation direction, which agrees perfectly well with the earlier estimates based on Fig. 10, for the noninteracting protons accelerated by the tightly focused fields. On the other hand, the mean exit kinetic energy of the accelerated protons from the PIC simulations is $K^*_{\rm exit} = 26.28 \pm 1.12$ MeV (i.e., a spread of about 4.3%). This also agrees well with the single- and many-particle calculation results, arrived at so far. Furthermore, the beam divergence (opening angle of the cone defined by the beam) can be estimated from Fig. 11 to be $\approx 0.3^\circ$. This value is much better than in other acceleration mechanisms such as RPA, where the beam divergence amounts to 10° [27]. However, it should be borne in mind that in Fig. 11 we used a mass-limited target. For targets of larger spatial dimensions such low divergence angles cannot be realized.

In all cases considered, the target dimensions are comparable to or lower than the laser wavelength. Such mass-limited targets may be more sensitive to fluctuations of the laser parameters, which arise in a realistic experimental implementation, than bulk targets. As an example, pulses produced by high-power laser systems are preceded by a pre-pulse. To study possible effects of a pre-pulse on the acceleration mechanism, we included a pre-pulse with a contrast ratio of 10^8 in the simulations. Such a contrast ratio may be considered typical (see, e.g., [51]); even a contrast of 10^{10} has been achieved [52]. The pre-pulse is assumed to be an unchirped plane wave with a Gaussian time profile. The FWHM pulse duration is taken to be $\tau = 2$ ps. The peak intensity corresponds to $I_0 = 1.315 \times 10^{14}$ W/cm^2. We have found that after the interaction with the pre-pulse the basic target shape remains maintained. After the passing of the pre-pulse, we let this slightly altered target interact with the main laser pulse, described by the parameters of Fig. 10. The exit kinetic energy after the interaction with the main pulse amounts to $K^*_{\rm exit} = 26.97 \pm 1.54$ MeV, which is almost identical to the values resulting from a simulation without a pre-pulse (see previous paragraph). Hence, we may conclude that our acceleration scheme is not significantly influenced by the inclusion of a pre-pulse with a typical contrast ratio.

We performed further simulations to assess the effect of variations of the initial size of the target. For an enlargement by a factor of up to 4 in the propagation direction, the exit kinetic energy and its spread do not change noticeably. However, a size increase by the same factor in the polarization direction leads to a change in the exit kinetic energy of up to 10% and to a larger energy spread (up to 6.9%). This can be explained by the transverse Gaussian intensity profile of the laser beam: Particles at different initial positions experience different field strengths and attain different kinetic energies.

TABLE I. Proton exit kinetic energies resulting from investigating the acceleration process in four, not totally unrelated, ways. The peak power is $P_0 = 1$ PW, and the remaining parameters are as follows: $\tau = 25$ fs, $w_0 = 1.8\lambda_0$, and $I_0 \simeq 1.965 \times 10^{22}$ W/cm^2 (plane wave) and $I_0 \simeq 1.981 \times 10^{22}$ W/cm^2 (tightly focused).

Case	b^*	$K^*_{\rm exit}$
A[a]	0.035224	27.02 MeV
B[b]	0.0289	26.09 MeV
C[c]	0.0289	25.95 ± 0.12 MeV
D[d]	0.035224	26.28 ± 1.12 MeV

[a]Single-particle accelerated by a plane-wave pulse.
[b]Single-particle accelerated by a tightly focused pulse
[c]Noninteracting proton ensemble accelerated by a tightly focused pulse.
[d]Preionized hydrogen plasma accelerated by a plane-wave pulse.

V. DISCUSSION AND MAIN CONCLUSIONS

The main objective of the present work has been to investigate the problem of proton acceleration by a high-power chirped laser pulse of short duration. One set of parameters has been the subject of four, not quite unrelated, methods of calculation. The set included the following: peak power $P_0 = 1$ PW, waist radius $w_0 = 1.8\lambda_0$, $\lambda_0 = 1$ μm, pulse duration $\tau = 25$ fs, and peak intensity $I_0 \simeq 1.965 \times 10^{22}$ W/cm^2. Single- and many-particle calculations have been performed. Acceleration from rest, of a single particle subjected to plane-wave and tightly focused Gaussian pulses, has been investigated first. This has been followed by many-particle simulations employing an ensemble of *noninteracting* protons and subjected to the fields of a tightly focused Gaussian pulse. Finally, PIC simulations have been carried out to study the dynamics of a preionized hydrogen plasma, with emphasis on the proton component. What is considered by us to be the most important results, namely, the exit particle kinetic energies turned up by each calculation (mean kinetic energies, in the many-particle cases considered) are collected in Table I. Good agreement between the four results is quite evident.

Good agreement between the results obtained on the basis of the plane-wave and tightly focused models is quite encouraging. Confidence in results based on the simple plane-wave treatments can be enhanced by improving the conditions which make its validity even more acceptable, namely, by relaxing the conditions on pulse duration and tight focusing only slightly, as will be exemplified shortly. For potential medical applications, like the use of protons in ion therapy, particle energies of a few hundred MeV are required. To highlight the possibility of laser acceleration of protons to such energies, the case employing a 1-PW peak-power pulse, of duration 350 fs and focused to $w_0 = 2.2\lambda_0$, has been considered along lines similar to the above. The results are collected in Table II. Only evolution with time (via η) of the kinetic energy, during interaction with the pulse, is displayed in Fig. 12. Agreement between the plane-wave and tightly focused models, especially as far as the exit kinetic energy is concerned, is almost perfect.

In addition to the two cases whose main results are collected in Tables I and II, many more have been investigated in this paper, which span pulse durations in the range of 25–800 fs,

TABLE II. Proton exit kinetic energies resulting from investigating the acceleration process in four, not totally unrelated, ways. The peak power is $P_0 = 1$ PW, and the remaining parameters are as follows: $\tau = 350$ fs, $w_0 = 2.2\lambda_0$, and $I_0 \simeq 1.315 \times 10^{22}$ W/cm^2 (plane wave) and $I_0 \simeq 1.326 \times 10^{22}$ W/cm^2 (tightly focused).

Case	b^*	K^*_{exit}
A[a]	0.00254644	252.31 MeV
B[b]	0.002508	253.73 MeV
C[c]	0.002508	252.46 ± 0.24 MeV
D[d]	0.00254644	242.39 ± 11.45 MeV

[a]Single-particle accelerated by a plane-wave pulse.
[b]Single-particle accelerated by a tightly focused pulse.
[c]Noninteracting proton ensemble accelerated by a tightly focused pulse.
[d]Preionized hydrogen plasma accelerated by a plane-wave pulse.

and result in exit kinetic energies from 26 MeV to over 850 MeV. Estimates of end results from those investigations, similar to the ones in the tables, may be read off Fig. 7.

In closing, readers interested in the prospects of utilizing radially polarized light for particle acceleration are advised to see [43]. Unfortunately, while more suited to the task of acceleration, radially polarized beams of the required intensity and power characteristics may not be available for laboratory experiments before a long while.

ACKNOWLEDGMENTS

Y.I.S. is supported by the Arab Fund for Economic and Social Development (State of Kuwait) through a Distinguished Scholar Award. B.J.G. acknowledges fruitful discussions with T. Pfeifer. The work of Z.H. is supported by the Alliance Program of the Helmholtz Association (HA216/EMMI).

APPENDIX: PULSE FORM REGULARIZATION

For a propagating electromagnetic pulse consisting of purely sinusoidally oscillating components, the integral over the pulse form has to vanish. As can be seen from Fig. 2(b) this is not the case for the pulse form introduced in Eq. (4).

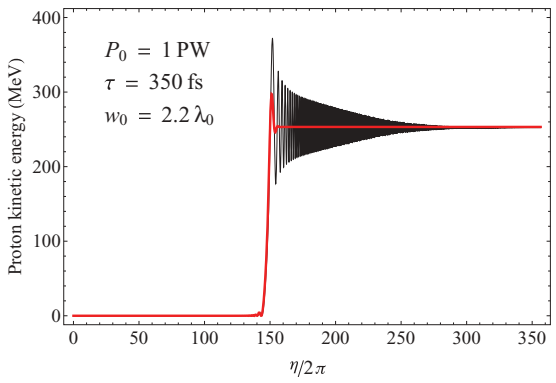

FIG. 12. (Color online) Evolution in η of the proton kinetic energy during interaction with a 350-fs pulse represented employing the plane-wave model (black) and the tightly focused fields (red or light gray).

Hence, it contains a static component which must be filtered out of its frequency spectrum.

To arrive at the frequency spectrum, denoted by $|\tilde{f}(\tilde{\eta})|^2$, one first calculates the Fourier transform $\tilde{f}(\tilde{\eta})$ of the pulse form $f(\eta)$. Let the Fourier transform conjugate of η be denoted by $\tilde{\eta}$. Note that for $z = 0$, $\eta = \omega_0 t$ and $\tilde{\eta} = \omega/\omega_0$. We work with the symmetric Fourier transform given by

$$\tilde{f}(\tilde{\eta}) \equiv \frac{1}{\sqrt{2\pi}} \int_{-\infty}^{\infty} f(\eta) e^{i\tilde{\eta}\eta} d\eta. \tag{A1}$$

For the specific pulse form $f(\eta)$ given in Eq. (4) the Fourier transform can be calculated fully analytically, provided $b > 0$, $\sigma > 0$, $\bar{\eta} > 0$. To save space the expression will not be quoted here.

To cancel the static component one may simply multiply $\tilde{f}(\tilde{\eta})$ by a filter function, for example,

$$g_1(\tilde{\eta}) = 1 - e^{-\frac{\tilde{\eta}^2}{2\Delta^2}}, \tag{A2}$$

where the width Δ (in units of ω/ω_0) introduces a smooth cutoff to the lower frequency part of the spectrum. The filtered spectrum ($|\tilde{f}_{\text{filt}}(\tilde{\eta})|^2$) may then be defined via

$$\tilde{f}_{\text{filt}}(\tilde{\eta}) \equiv g_1(\tilde{\eta}) \tilde{f}(\tilde{\eta}). \tag{A3}$$

The filtered pulse form in η space is then the inverse Fourier transform,

$$f_{\text{filt}}(\eta) \equiv \frac{1}{\sqrt{2\pi}} \int_{-\infty}^{\infty} \tilde{f}_{\text{filt}}(\tilde{\eta}) e^{-i\tilde{\eta}\eta} d\tilde{\eta}. \tag{A4}$$

Now one may show that the integral over the regularized pulse form $f_{\text{filt}}(\eta)$ vanishes, as follows:

$$\begin{aligned} \int_{-\infty}^{\infty} f_{\text{filt}}(\eta) d\eta &= \int_{-\infty}^{\infty} \frac{1}{\sqrt{2\pi}} \int_{-\infty}^{\infty} \tilde{f}_{\text{filt}}(\tilde{\eta}) e^{-i\tilde{\eta}\eta} d\tilde{\eta} d\eta \\ &= \sqrt{2\pi} \int_{-\infty}^{\infty} \tilde{f}_{\text{filt}}(\tilde{\eta}) \delta(\tilde{\eta}) d\tilde{\eta} \\ &= \sqrt{2\pi}\, \tilde{f}_{\text{filt}}(\tilde{\eta})|_{\tilde{\eta}=0} = 0. \end{aligned} \tag{A5}$$

The strong positive signature at $\eta^*/2\pi \simeq 8.21$ (corresponding to the filtered out zero frequency) gets compensated by a quasistatic tail of a slightly negative amplitude which tends to zero asymptotically. To choose a reasonable filter width one is guided by the need to maintain the exit kinetic energy gain. In Fig. 7 we compare the energy gained by a proton calculated using the original pulse form (black line) and the filtered pulse form (red line). The exit kinetic energy corresponds to 27 MeV for the original pulse form and to 25.5 MeV for the filtered pulse, for the applied filter width $\Delta = 0.0002$. It can be seen that both lines coincide, and only start to deviate towards the end. This may be attributed to the slightly negative tail added to the pulse form by the filtering procedure. One might argue that for a longer interaction interval the kinetic energy gain may be decreased further. While this holds true for the plane-wave model, this is certainly not true for the (more realistic) tightly focused fields. Here the particle gets ejected from the focal region before it is decelerated by the quasistatic negative tail.

The above filtering procedure also amounts to damping a frequency band around $\omega = 0$ of width $\delta\omega = \omega_0\Delta = (2\pi/T)\Delta$, where T is one laser field cycle. Assuming that the pulse duration τ is equivalent to N_f cycles, then $N_f = \tau/T = 7.5$, for $\tau = 25$ fs and $\lambda = 1\ \mu$m. Therefore, $\delta\omega = (0.003\pi)\tau^{-1}$.

[1] F. Watt, A. A. Bettiol, J. A. Van Kan, E. J. Teo, and M. B. H. Breese, Int. J. Nanosci. **4**, 269 (2005).
[2] D. Winston *et al.*, Nano Lett. **11**, 4343 (2011).
[3] S. E. Combs *et al.*, Cancer **115**, 1348 (2009).
[4] D. Schardt, T. Elsässer, and D. Schulz-Ertner, Rev. Mod. Phys. **82**, 383 (2010).
[5] S. Fritzler, K. Ta Phuoc, V. Malka, A. Rousse, and E. Lefebvre, Appl. Phys. Lett. **83**, 3039 (2003).
[6] X. Y. Peng, J. Zhang, J. Zheng, Z. M. Sheng, M. H. Xu, Z. Y. Zheng, T. J. Liang, Y. T. Li, Q. L. Dong, X. H. Yuan, Y. J. Li, and H. M. Li, Phys. Rev. E **74**, 036405 (2006).
[7] O. Jäkel, D. Schulz-Ertner, C. P. Karger, P. Heeg, and J. Debus, Nucl. Instrum. Methods Phys. Res., Sect. B **241**, 717 (2005); S. E. Combs *et al.*, Cancer **115**, 1348 (2009); O. Jäkel, M. Krämer, C. P. Karger, and J. Debus, Phys. Med. Biol. **46**, 1101 (2001); [http://www.gsi.de/portrait/beschleunigeranlage_e.html]; [http://www.wanjiehospital.com/proton/program.htm].
[8] B. M. Hegelich *et al.*, Nature (London) **439**, 441 (2006).
[9] H. Schwoerer *et al.*, Nature (London) **439**, 445 (2006).
[10] J. Fuchs *et al.*, Nature Physics **2**, 48 (2006).
[11] L. Robson *et al.*, Nature Physics **3**, 58 (2007).
[12] R. A. Snavely *et al.*, Phys. Rev. Lett. **85**, 2945 (2000).
[13] S. Karsch, S. Dusterer, H. Schwoerer, F. Ewald, D. Habs, M. Hegelich, G. Pretzler, A. Pukhov, K. Witte, and R. Sauerbrey, Phys. Rev. Lett. **91**, 015001 (2003).
[14] L. Romagnani *et al.*, Phys. Rev. Lett. **95**, 195001 (2005).
[15] T. Tajima and J. M. Dawson, Phys. Rev. Lett. **43**, 267 (1979).
[16] A. J. Mackinnon, M. Borghesi, S. Hatchett, M. H. Key, P. K. Patel, H. Campbell, A. Schiavi, R. Snavely, S. C. Wilks, and O. Willi, Phys. Rev. Lett. **86**, 1769 (2001).
[17] G. A. Mourou *et al.*, Rev. Mod. Phys. **78**, 309 (2006).
[18] A. Maksimchuk, S. Gu, K. Flippo, D. Umstadter, and V. Y. Bychenkov, Phys. Rev. Lett. **84**, 4108 (2000).
[19] M. Passoni and M. Lontano, Phys. Rev. Lett. **101**, 115001 (2008).
[20] S. C. Wilks, A. B. Langdon, T. E. Cowan, M. Roth, M. Singh, S. Hatchett, M. H. Key, D. Pennington, A. MacKinnon, and R. A. Snavely, Phys. Plasmas **8**, 542 (2001).
[21] T. Esirkepov, M. Borghesi, S. V. Bulanov, G. Mourou, and T. Tajima, Phys. Rev. Lett. **92**, 175003 (2004).
[22] M. Passoni, L. Bertagna, and A. Zani, New J. Phys. **12**, 045012 (2010).
[23] V. T. Tikhonchuk, Nucl. Instrum. Methods A **620**, 1 (2010).
[24] T. V. Liseykina, M. Borghesi, A. Macchi, and S. Tuveri, Plasma Phys. Controlled Fusion **50**, 124033 (2008).
[25] I. V. Pogorelsky, V. Yakimenko, M. Polyanskiy, P. Shkolnikov, M. Ispiryan, D. Neely, P. McKenna, D. Carroll, Z. Najmudin, and L. Willingale, Nucl. Instrum. Methods Phys. Res., Sect. A **620**, 67 (2010).
[26] C. A. J. Palmer, N. P. Dover, I. Pogorelsky, M. Babzien, G. I. Dudnikova, M. Ispiriyan, M. N. Polyanskiy, J. Schreiber, P. Shkolnikov, V. Yakimenko, and Z. Najmudin, Phys. Rev. Lett. **106**, 014801 (2011).
[27] B. Qiao, M. Zepf, M. Borghesi, and M. Geissler, Phys. Rev. Lett. **102**, 145002 (2009).
[28] A. Henig *et al.*, Phys. Rev. Lett. **103**, 245003 (2009).
[29] A. Macchi, S. Veghini, and F. Pegoraro, Phys. Rev. Lett. **103**, 085003 (2009).
[30] S. V. Bulanov, E. Y. Echkina, T. Z. Esirkepov, I. N. Inovenkov, M. Kando, F. Pegoraro, and G. Korn, Phys. Rev. Lett. **104**, 135003 (2010).
[31] Y. I. Salamin, Opt. Lett. **32**, 3462 (2007).
[32] Y. I. Salamin, Z. Harman, and C. H. Keitel, Phys. Rev. Lett. **100**, 155004 (2008).
[33] Z. Harman, Y. I. Salamin, B. J. Galow, and C. H. Keitel, Phys. Rev. A **84**, 053814 (2011).
[34] B. J. Galow, Z. Harman, and C. H. Keitel, Opt. Express **18**, 25950 (2010).
[35] B. J. Galow, Y. I. Salamin, T. V. Liseykina, Z. Harman, and C. H. Keitel, Phys. Rev. Lett. **107**, 185002 (2011).
[36] E. Goulielmakis *et al.*, Opt. Lett. **33**, 1407 (2008).
[37] R. K. Shelton *et al.*, Science **293**, 1286 (2001).
[38] H.-S. Chan *et al.*, Science **331**, 1165 (2011).
[39] K. P. Singh, Appl. Phys. Lett. **87**, 254102 (2005).
[40] F. Sohbatzadeh, S. Mirzanejhad, and M. Ghasemi, Phys. Plasmas **13**, 123108 (2006).
[41] F. Sohbatzadeh, S. Mirzanejhad, and H. Aku, Phys. Plasmas **16**, 023106 (2009).
[42] F. Peano *et al.*, IEEE Trans. Plasma Sci. **36**, 1857 (2008).
[43] J.-X. Li, Y. I. Salamin, B. J. Galow, and C. H. Keitel, Phys. Rev. A **85**, 063832 (2012).
[44] F. Peano *et al.*, Phys. Plasmas **14**, 056704 (2007).
[45] B. Ramakrishna, M. Murakami, M. Borghesi, L. Ehrentraut, P. V. Nickles, M. Schnürer, S. Steinke, J. Psikal, V. Tikhonchuk, and S. Ter-Avetisyan, Phys. Plasmas **17**, 083113 (2010).
[46] S. Ter-Avetisyan, M. Schnürer, P. V. Nickles, M. Kalashnikov, E. Risse, T. Sokollik, W. Sandner, A. Andreev, and V. Tikhonchuk, Phys. Rev. Lett. **96**, 145006 (2006).
[47] S.-W. Bahk *et al.*, Opt. Lett. **29**, 2837 (2004).
[48] [http://www.extreme-light-infrastructure.eu/pictures/ELI - scientific-case-id17.pdf].
[49] [http://www.hiperlaser.org/docs/tdr/HiPERTDR2.pdf].
[50] Y. I. Salamin, Appl. Phys. B **86**, 319 (2007).
[51] M. Veltcheva, A. Borot, C. Thaury, A. Malvache, E. Lefebvre, A. Flacco, Lopez-R. Martens, and V. Malka, Phys. Rev. Lett. **108**, 075004 (2012).
[52] H. Kiriyama *et al.*, Appl. Opt. **49**, 2105 (2010).